ORIGINAL ARTICLE

Biosorption of acid brown 14 dye to mandarin-CO-TETA derived from mandarin peels

Tarek M. Eldeeb[1] · Uyiosa O. Aigbe[2] · Kingsley E. Ukhurebor[3] · Robert B. Onyancha[4] · Mohamed A. El-Nemr[5] ·
Mohamed A. Hassaan[1] · Otolorin A. Osibote[2] · Safaa Ragab[1] · Benedict Okundaye[6] · Vincent A. Balogun[7] ·
Ahmed El Nemr[1] (ID)

Abstract

Several agronomic waste-materials are presently being widely used as bio-adsorbents for the treatment of toxic wastes such as dyes and heavy metals from industrial activities, which has resulted in critical global environmental issues. Therefore, there is a need to continue searching for more effective means of mitigating these industrial effluents. Synthetic aromatic dyes such as Acid Brown (AB14) dye are one such industrial effluent that is causing a serious global issue owing to the huge amount of these unsafe effluents released into the ecosystem daily as contaminants. Consequently, their confiscation from the environment is critical. Hence, in this study, Mandarin-CO-TETA (MCT) derived from mandarin peels was utilized for the removal of AB14 dyes. The synthesized biosorbent was subsequently characterized employing FTIR, TGA, BET, and SEM coupled with an EDX. The biosorption of this dye was observed to be pH-dependent, with the optimum removal of this dye being noticed at pH 1.5 and was ascribed to the electrostatic interaction between the positively charged sites on the biosorbent and the anionic AB14 dye. The biosorption process of AB14 dye was ideally described by employing the pseudo-second-order (PSO) and the Langmuir (LNR) models. The ideal biosorption capacity was calculated to be 416.67 mg/g and the biosorption process was indicative of monolayer sorption of AB14 dye to MCT biosorbent. Thus, the studied biosorbent can be employed as a low-cost activated biomass-based biosorbent for the treatment of AB14 dyes from industrial activities before they are further released into the environment, thus mitigating environmental contamination.

Keyword Acid Brown 14 dye; Biosorption; Mandarin peels; Pollution; Wastewater, Mandarin-CO-TETA

1 Introduction

The world over, the problems of ecological annihilations that are prompting several environmental effluences (toxic wastes) and damaging the natural resources as a result of

the growth in industrial activities and a vast increase in the population, in addition to the incessant evolution of technological advancement, is now a critical menace to the human race and its immediate environment [1–6]. A larger part of these environmental toxic wastes is from industrial activities such as dyes [7–10], heavy metals (HMs) [11, 12], wastewater (effluents) [13, 14], crude oil spills, and gas flares [6, 15, 16]. These rising environmental effluences from industrial activities are one of the greatest causes of the harmful environmental, climatic, and health difficulties that are antagonizing both the terrestrial, atmospheric, and aquatic ecosystems [5, 6, 11].

Wastewaters (effluents) caused by the production activities of the textile and some other industries, such as printing and leather processing industries, are identified to have a substantial amount of poisonous aromatic dyes, particularly the azo dyes such as Acid Brown 14 (AB14). The coloured wastewater (effluents) released during the production

✉ Ahmed El Nemr
  ahmedmoustafaelnemr@yahoo.com;
  ahmed.m.elnemr@gmail.com

Extended author information available on the last page of the article

activities of the textile industries into the environment is one of the dramatic causes of environmental contamination as well as a perturbation in the aquatic ecosystem (water bodies) [17]. These wastewaters (effluents) contain complex concentrations of dye composites like AB14, which are typically generated from various sources, particularly in the textile, printing, and leather processing industries. These dye composites are essentially non-biodegradable and have adverse effects on living organisms and the environment due to their harmfulness [18]. Hence, these effluents are identified to have a substantial amount of poisonous aromatic dyes, particularly azo dyes. As stated earlier, the coloured effluents released during the production activities of the textile, printing, and leather processing industries into the environment are one of the most dramatic sources of esthetical contamination as well as a perturbation in the aquatic ecosystem [17]. The AB14 ($C_{26}H_{16}N_4Na_2O_8S_2$) is a distinctive pollutant, and it is one of the widespread commercial azo dyes [17, 18]. The chemical/molecular structural illustration of the AB14 is shown in Fig. 1.

The confiscation of these dye composites, which are essentially non-biodegradable from water bodies, is critical to living organisms and the ecosystem. Over the years, several procedures are adsorption [13, 18], oxidation procedures (photocatalysis) [18–21], chemical precipitation [22], coagulation/flocculation [18], reverse-osmosis [12], ion exchange [11], membrane filtration [11], biological treatment and biological processes [18, 23], advanced oxidations [24–28], etc. The adsorption process is reported to be more effective owing to its simplicity, effectiveness, and the certainty that it does not generate sludge, thus warranting a safe ecosystem [29–33]. The adsorption process is a unique procedure for the sequestration of effluents from water bodies by precisely putting them on the surface of the bio-adsorbent [34]. This process is cheaper compared to other procedures, especially if the bio-adsorbent is common (easily available) without any prior treatment before its utilization in the confiscation and treatment of effluents [13]. Also, its suitability and simplicity in terms of operation and design have made the adsorption process outstanding [35, 36]. Besides, most biomass-based adsorbents have the advantage over the conventional treatment methods for dyes by mitigating some specific limitations (such as those related

to operation effectiveness, overall cost, energy, and generation of noxious consequences) of the conventional treatment. Among the various existing adsorbents, activated biomass-based treatments are believed to be the most recently utilized for the removal of dyes and effluents [35, 37].

Evidently, several agronomic waste materials from crops, plants, or fruits such as leaves, stems, peels, and other waste parts of some inexpensive and available crops, plants, or fruits (such as waste from sugarcane, maize, jackfruit, rice, mango, orange, cloves, coconut, palm fruits, watermelon, etc.) are presently being extensively used as bio-adsorbents for the sequestration, management, and treatment of toxic wastewaters (contaminated waters) from industrial activities by dyes, HMs, and other toxic substances that subsequently find their way into various water bodies (aquatic ecosystems) [13, 38, 39]. According to reports, the cells of these crops, plants, or fruits are made up of tannin, lignin, and cellulose, all of which have enormous potential for absorbing dyes and HMs ions [6, 9, 40]. Hence, there is a need to continue searching for more effective means of mitigating these industrial effluents. Therefore, evolving more cheap and effective confiscation techniques is a continuous postulation [36, 41]. Consequently, in this present study, the prospects of further investigating the potential of using inexpensive and available crops, plants, or fruits as bio-adsorbents for the confiscation of dyes, specifically the AB14, which is one of the toxic dyes from water bodies (aquatic ecosystems), were emphasized. The inexpensive and available fruit that was utilized as bio-adsorbent for this study was the peels from the fruit of the "mandarin (mandarin or mandarine) orange (*Citrus reticulata*), which is regarded as a distinct kind of orange (see Fig. 2) [42].

Hence, this study explores the prospects of using a new biosorbent prepared from mandarin peels an agronomic waste material for activated biomass-based biosorbent production. The prepared activated biomass-based biosorbent was oxidized to have epoxide and COOH groups which reacted with triethylenetetramine (TETA) to form modified Mandarin-CO-TETA (MCT) for the sequestration of AB14 dye from the aquatic environment. The batch adsorption studies for the sequestration of AB14 dye from industrial toxic wastes were characterized and the evaluation of the
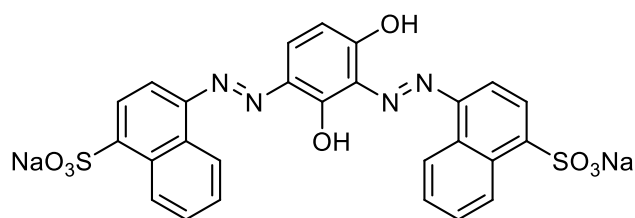

Fig. 1 Chemical/molecular structure of AB14 dye [18]

Fig. 2 The fruit, along with mandarin orange peels (*Citrus reticulata*)

optimization of the different parameters and factors, in addition to the estimation of the thermodynamics, kinetics, and adsorption isotherms were fundamentally deliberated. The rationale for this study was to establish the use of MCT as one of the effective activated biomass-based biosorbents for the removal of AB14 dye via the adsorption procedure from industrial effluents before they are further released into the environment, and this will be of great significance in mitigating environmental contamination from industrial effluents.

2 Materials and methods

2.1 Materials

Mandarin orange (*Citrus reticulata*) peels obtained from a local market were used for the production of MCT. Sulfuric acid (H_2SO_4, M.W. = 98.07 g, 99%) and Acid Browen 14 (AB14) dye ($C_{26}H_{16}N_4Na_2O_8S_2$) were supplied from Sigma-Aldrich. AB14 dye standard stock solution was prepared by dissolving one gram of dye in a liter of distilled water. H_2O_2 (50%) and TETA were obtained from Sigma-Aldrich. A digital UV/Visible spectrophotometer (SPEKOL1300) using glass cells with a 1 cm optical path, a JSOS-500 shaker, and a JENCO-6173 pH meter was used. As reported by Tran et al. [43], different nitrogen sources, derived from "acetonitrile, nitrogen gas, ethylenediamine amines, ammonia, urea, dimethylformamide, ammonia gas, pyridine, melamine, 2-amino-4,6-dichloro-s-triazine, polyazomethineamide, benzylamine, and TETA," have been employed for producing nitrogen-doped carbon-based biosorbents. Among the aforementioned, TETA has been extensively utilized as an effective cationic surface-active agent (surfactant) for modifying the surface of biosorbents [43].

2.2 Preparation of the activated biomass-based biosorbent

Mandarin orange (*Citrus reticulata*) peels were properly washed many times with water to eliminate dust and then dried for 48 h at 105 °C. Crushed and ground dried Pea peels were used in this recipe. For this experiment, 300 g of crushed mandarin peels were boiled for 3 h in 1.5 L of 50% of H_2SO_4 in a refluxed system (130 °C), after which they were diluted with distilled water, filtered, and washed with water until the filtrate became neutral, and then washed with ethanol and dried overnight at 105 °C and weighed to produce 125 g. The processes of sulphonation occurred as a result of this method of preparation. The mandarin-activated biomass-based biosorbent produced (100 g) as a result of this reaction was suspended in 300 ml of 50% H_2O_2 and heated at 70 °C for 30 min. The oxidized mandarin activated biomass-based biosorbent was filtered, washed with water

and dried overnight at 105 °C and weighed to give 85 g. The oxidized mandarin activated biomass-based biosorbent (30 g) was then heated in a 100 mL solution of TETA for 2 h in a refluxed system. The reaction mixture was filtered and rinsed twice with distilled water and ethanol and dried at 70 °C overnight to give 37 g. TETA was added to the product's label, which read MCT.

2.3 Batch adsorption experimental

A stock solution of AB14 dye (1000 mg L^{-1}) was obtained by dissolving 1.0 g of AB14 dye in 1 L of pure water, and this solution was diluted to the desired concentrations for the calibration standard curve and adsorption tests. The adsorption capabilities, thermodynamic and kinetic characteristics of MCT were determined using batch adsorption studies. A series of Erlenmeyer flasks (300 mL) was shaken at 200 rpm for a specified duration with 100 mL of various concentrations of AB14 dye solution and varying volumes of MCT. With 0.1 M HCl or 0.1 M NaOH, the pH of the sample was changed to the appropriate levels. Concentration measurement of AB14 dye was performed by taking 1 mL sample from the solution in the Erlenmeyer flask and separating it from the adsorbent, at various intervals and equilibrium. The adsorption experiments were repeated three times and only the mean values were used in the thermal and kinetic analyses for simplicity. The concentration of AB14 dye was measured using spectrophotometry $\lambda_{max} = 461$ nm. The equilibrium adsorption capacities (q_e) were estimated using Eq. (1):

$$q_t = \frac{(C_0 - C_t)}{W} \times V \tag{1}$$

where the adsorption capacity (q_t) (mg adsorbate/g adsorbent) is the adsorbent's ability to remove AB14 dye from a solution at a certain time. C_0 (mg/L) is the initial concentration of AB14 dye; C_t (mg/L) is the residual concentration of
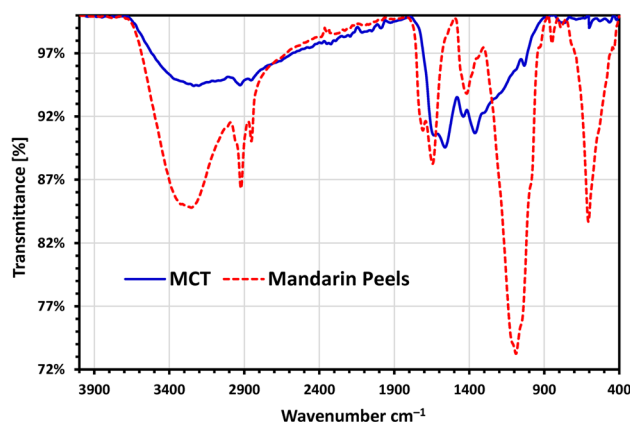

Fig. 3 FTIR analysis of mandarin peels and MCT adsorbent

the AB14 dye after the adsorption process had been completed for a given time. The following equation (2) can be used to calculate the elimination % of AB14 dye from an aqueous solution.

$$Removal(\%) = \frac{(C_0 - C_t)}{C_0} \times 100 \qquad (2)$$

The influence of pH on AB14 dye adsorption was examined by mixing 0.1 g of the adsorbent with 100 mL of AB14 dye solution at a concentration of 100 mg/L for MCT (0.1 g) with initial pH values varying between 1.5 and 12. 0.1 M HCl and 0.1 M NaOH solutions were used to modify the pH levels. At 25 °C, the suspensions were agitated at 200 rpm for 180 min before being sampled for AB14 dye measurement.

For the isotherm investigation, 100 mL of AB14 dye solutions were mixed at 200 rpm for 3 h at 25 °C with varying initial concentrations of AB14 dye solutions (100–400 mg/L) and various amounts of MCT (25 to 125 mg).

At 25 °C, the effect of adsorbent dosage and contact time on AB14 dye removal was investigated by shaking 100 mL of initial AB14 dye concentration for MCT with varied adsorbent dosages of (25, 50, 75, 100, and 125 mg) at different interval times at 25 °C.

Fig. 4 **A** Adsorption desorption graph, **b** BET analysis graph, and **c** BJH analysis graph of MCT
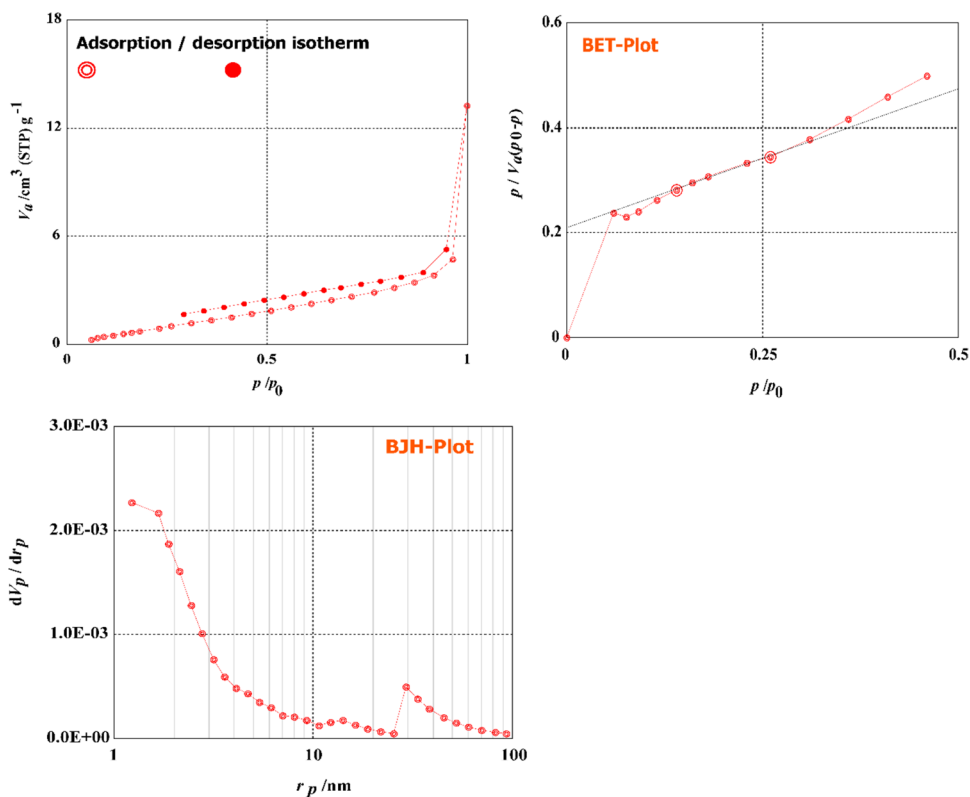
Fig. 5 SEM image of MCT magnification at ×800 under high vacuum
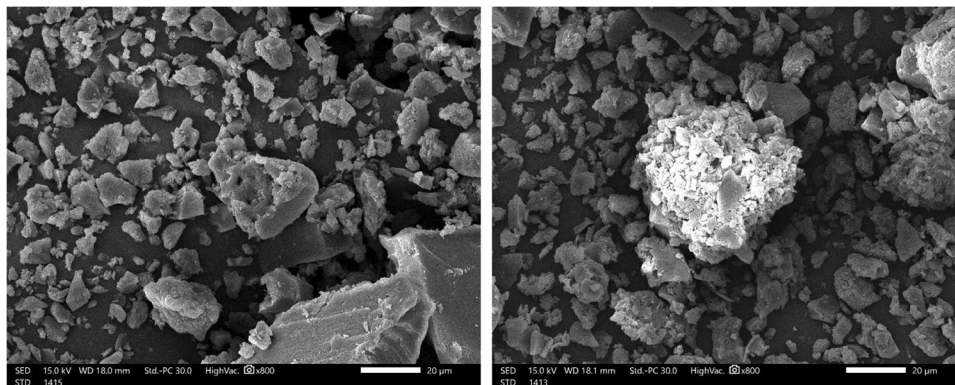
2.4 MCT characterization

The adsorption–desorption isotherm of N_2 on MCT was calculated at the boiling point of nitrogen gas. The surface area and pore analyzer (BELSORP – Mini II, BEL Japan, Inc.) was used to assess the BET surface area (S_{BET}) of the activated biomass-based biosorbent using nitrogen adsorption at 77 K [44, 45]. The BET plot was used to calculate surface area (S_{BET}) (m^2/g), monolayer volume (V_m) (cm^3 (STP) g^{-1}), total pore volume (p/p_0) (cm^3/g), mean pore diameter (nm), and energy constant (C) for the isotherm. The following equation (3) was used to compute the average pore radius.

$$r(nm) = \frac{2V_T(mLg^{-1})}{a_{S,BET}(m^2g^{-1})} \times 1000 \tag{3}$$

To determine the mesopore surface area (S_{mes}), micropore surface area (S_{mi}), mesopore volume (V_{mes}), and micropore volume (V_{mi}) of MCT, the Barrett-Joyner–Halenda (BJH) method was used by using the BELSORP analysis program software. The pore size distribution is calculated from the desorption isotherm using the BJH method [46].

The surface morphology of the MCT sample was investigated using a Scanning Electron Microscope (SEM) (QUANTA 250) in conjunction with an Energy Dispersive X-ray Spectrometer (EDX) for elemental analysis.

The functional groups on the MCT surface were investigated using Fourier Transform Infrared (FTIR) spectroscopy (VERTEX70) and ATR unit model V-100.

Thermal analyzes were carried out using the SDT650-Simultaneous Thermal Analyzer device at a temperature range of 25 to 1000 °C, at a temperature increase rate of 5 °C/min.

3 Results and discussions

3.1 The characteristics of MCT

Fourier Transform Infrared Spectroscopy (FT-IR) was used to analyse the generated activated biomass-based biosorbent sample to detect changes in the functional groups of the sample. The raw mandarin peels and MCT FT-IR spectra are shown in Fig. 3. Specifically, the strong band at 3252.8 cm^{-1} corresponds to the O–H stretching vibration that existed in mandarin peels, whereas the broad adsorption peak about 3237.5 cm^{-1} is indicative of the presence of the –OH group of glucose and the –NH of the amino group in the MCBT (Fig. 3). The presence of this new band suggested that the amino group had been introduced into the activated biomass-based biosorbent structure. According to this theory, the –CH_2 stretching vibration that existed in mandarin peels and the MCT existed at 2922.6–2853.1 cm^{-1} and 298.4–2855.0 cm^{-1},
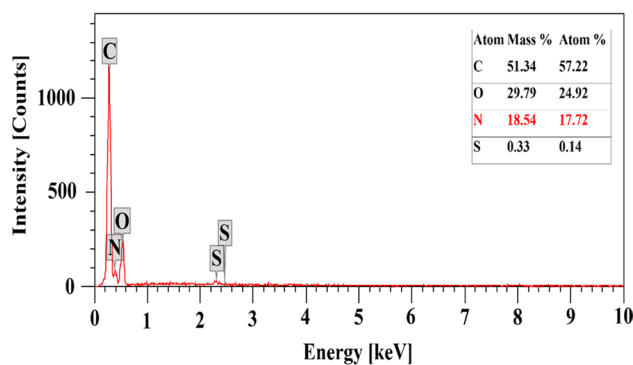

Fig. 6 EDX analysis of MCT prepared from mandarin peels

respectively. There is no adsorption peak at about 1709.9 cm^{-1}, demonstrating that the C=O stretching of the carboxyl group that appeared in mandarin peels, but disappeared in the prepared activated biomass-based biosorbent MCT (Fig. 3). The presence of the band at 1645 cm^{-1} in mandarin peels and at 1634.95 cm^{-1} in MCT indicated the presence of amide groups in both materials. In MCT, the N–H stretching vibration in fatty amine or aromatic secondary amine was observed at a frequency of 1562.4 cm^{-1}, indicating that TETA modification may have increased the N–H functional group of MCT. The adsorption peak at 1417.3 cm^{-1} indicates the presence of the C–O functional group in mandarin peels, whereas the strong adsorption peaks at 1439.9 and 1362.4 cm^{-1} were attributable to the stretching vibration of the –N=C=O group in MCT. The appearance of this new peak on MCT, which was caused by nitrogen-containing functional groups, indicates that amino groups were successfully introduced following the treatment with TETA. The band at 1033.6 cm^{-1} represents the C–O–H functional group in MCT while it is strong in mandarin peels at 1089.2 cm^{-1}. Furthermore, it seems there was an obvious difference between mandarin peels and MCT in the peak strength
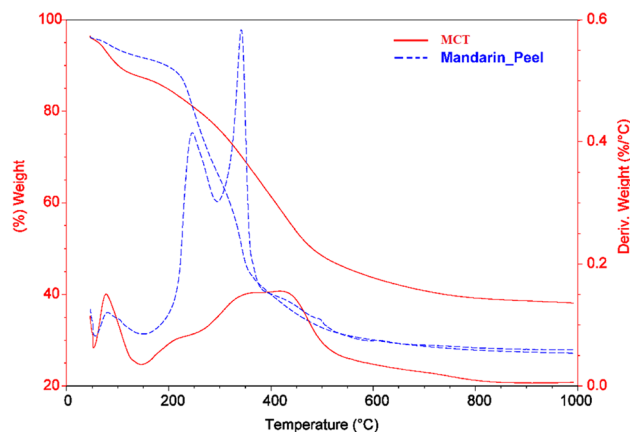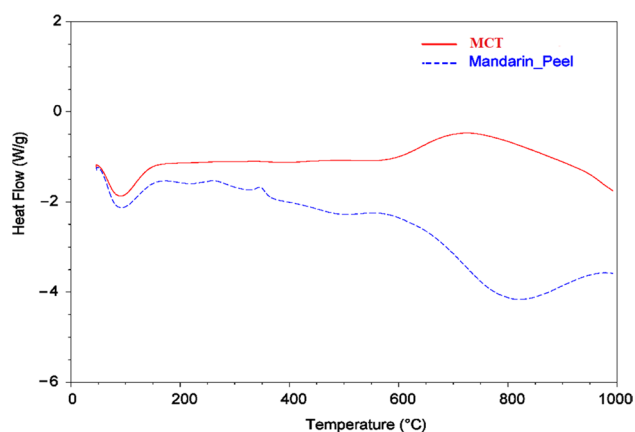

Fig. 7 TGA and DTA analyses of raw mandarin peels and MCT

Fig. 8 DSC analysis of raw mandarin peels and MCT

of 1030–1090 cm^{-1}, indicating TETA modification could affect the C–O–H functional group of MCT (Fig. 3). Also, the OH vibration that appeared at 606.1 cm^{-1} in mandarin peels was completely disappeared in the prepared adsorbent MCT.

The textural parameters of the MCT were computed using the (BET) and (BJH) methods and are shown in Fig. 4. They include the BET-specific surface area, total pore volume, mean pore diameter, monolayer volume, mesopore area, mesopore volume, and mesopore distribution peak. As illustrated in Fig. 4, MCT had a BET-specific surface area of 5.88 m^2/g and a monolayer volume of 1.3519 cm^3(STP)/g. MCT had a total pore volume of 0.017 cm^3/g and a mean pore diameter of 11.715 nm (mesopores). MCT has a mesosurface area of 6.1776 m^2/g and a mesopore volume of 0.01835 cm^3/g. MCT had a mesopore distribution peak of 1.22 nm. The pores in the manufactured modified activated biomass–based

biosorbent have been reported to be closed by the amine functional groups [30, 31].

SEM micrographs of the MCT were examined. Figure 5 shows the surface morphology of MCT and according to the image, most of the pores and caves had been blocked by the amine-creating active sites [30, 31]. The images characterization showed an irregular form, uneven edge agglomeration, and nonporous surface [47], which may be occurred as a result of surface amination with TETA. This nonporous surface structure may explain the lower surface area obtained from the BET analysis.

The EDX analysis was carried out for the MCT for its chemical composition. The chemical composition of MCT was reported in Fig. 6, which showed the EDX analysis of MCT proved the presence of 18.54% sample weight for nitrogen element. The major elements in the MCT were carbon (51.34%) followed by oxygen atoms (29.79%) and nitrogen (18.54%). A small amount of sulphur atom (0.33%) was recorded as a result of the dehydration step with 50% H$_2$SO$_4$.

The thermogravimetric profile of the raw materials' mandarin peels and MCT as a function of temperature is shown in Fig. 7. The decomposition of the raw material mandarin peels occurs in four processes, whereas the decomposition of the MCT occurs in two steps, as shown in Fig. 7. The first step, which occurs between 50 and 150 °C, results in the loss of surface-bound water and moisture in the sample, with weight losses of 4.5 and 8.85%, respectively, for the raw material mandarin peels and MCT. In the second weight-loss stage, mandarin peels lost 25.27% at 150–300 °C and MCT losing 49.33% at 150–1000 °C, respectively. At 300–385 °C, the mandarin peel loses about 25.04% of its weight in the third weight-loss stage followed by losing 14.23% of its weight in the fourth and final weight-loss stage between 385 and 1000 °C [30, 31].
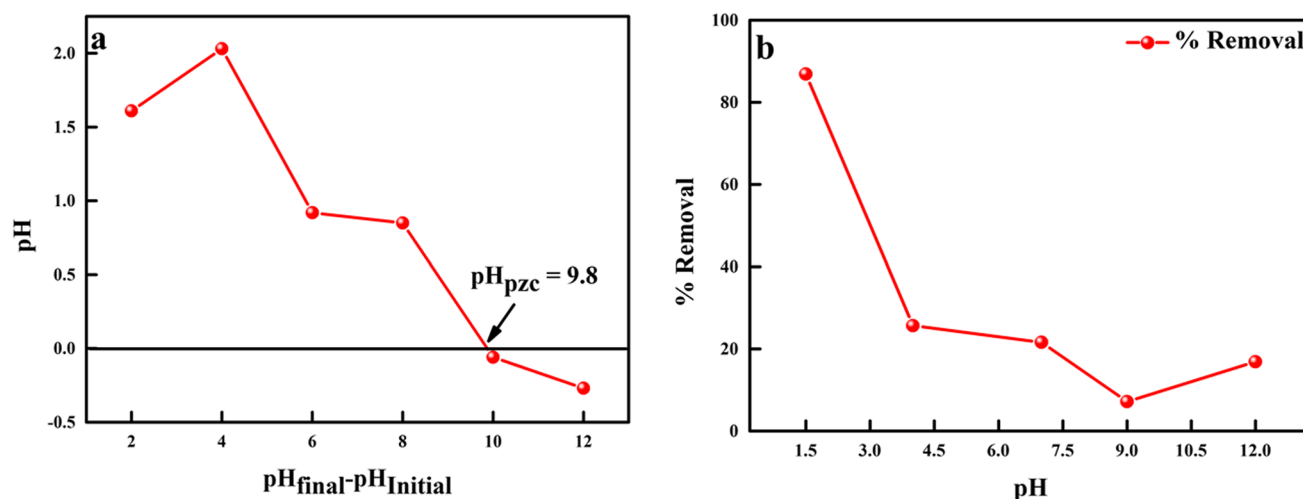
Fig. 9 **A** Assessed pH$_{pzc}$ of the MCT biosorbent and **b** impact of pH on the biosorption of AB14 dye

Differential thermal analysis (DTA) can be used solely for identification purposes, although it is most commonly employed for phase diagram determination, heat change measurements, and decomposition in various atmospheres (Fig. 7). The DTA curve of the mandarin-peels sample exhibits three peaks at a temperature of flow Tf (80.19, 243.82, and 342.32 °C). However, the pyrolysis of the mandarin peels shows three well-resolved degradation peaks. The DTA analysis of the MCT sample showed manly two well-resolved degradation peaks at a temperature of flow Tf

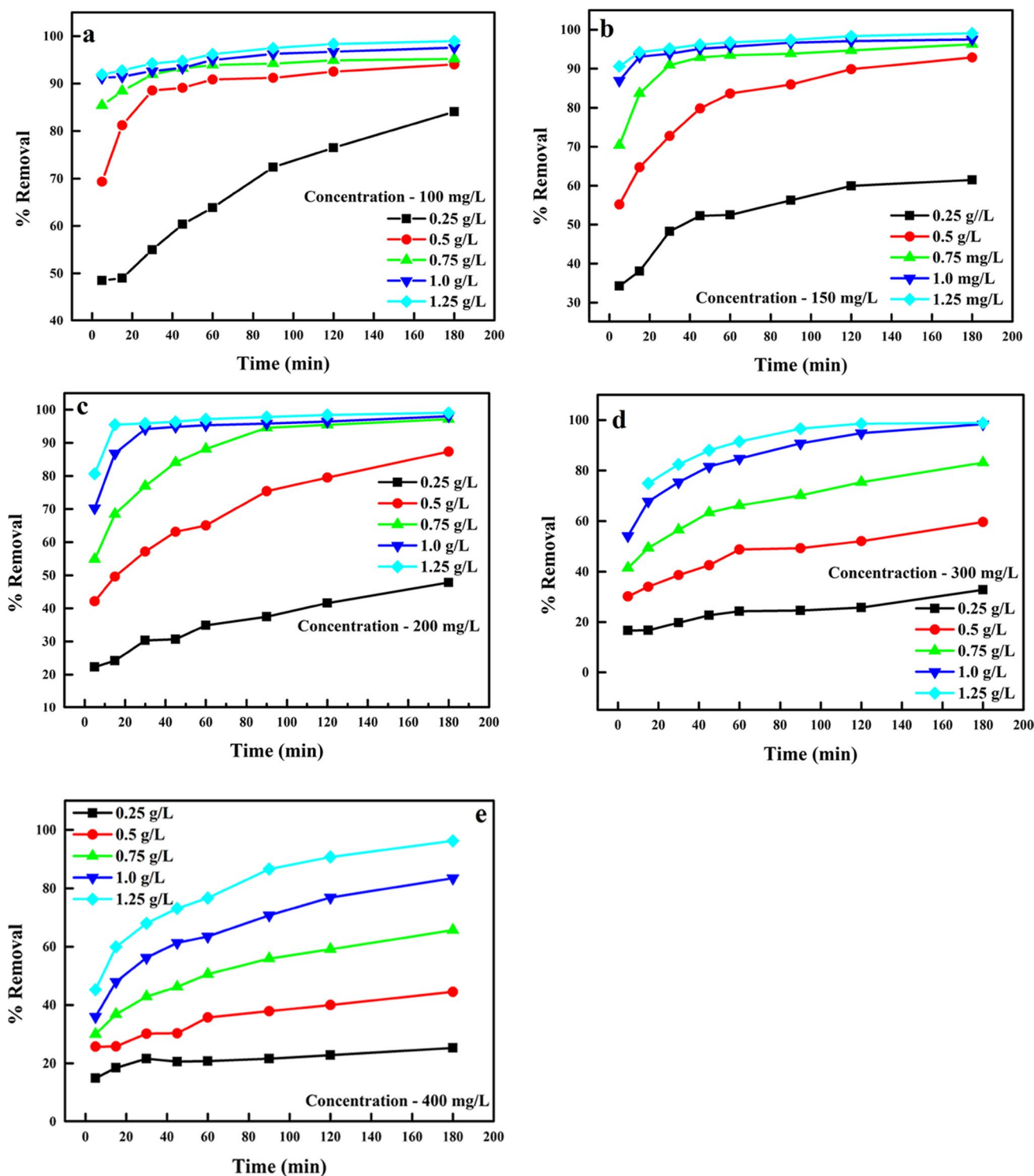**Fig. 10** Impact of biosorbent dosage at initial AB14 dye concentrations of **a** 100 mg/L, **b** 150 mg/L, **c** 200 mg/L, **d** 300 mg/L, and **e** 400 mg/L

(77.94, 416.87 °C), and onset points at 57.2, and 211.68 °C. This proved that the stability of the MCT sample increased by modification than mandarin peels [30, 31].

Using differential scanning calorimetry (DSC), thermal transitions can be used to compare materials. Figure 8 illustrates the DSC analyses of raw mandarin peels and MCT. Both of the samples had crystallisation temperatures T_C below 100 °C (89.05 and 90.93 °C, respectively), which can be attributed to water molecule crystallisation. Two other exothermic phase transitions were reported for the DSC analysis of mandarin peels at 263.73 and 347.82 °C. The other crystallisation temperature T_C of raw mandarin peels was found to be at 482.19 and 807.41 °C using DSC. Two other phase transitions were reported for the DSC of MCT at 393.04 °C and 728.57 °C as endothermic and exothermic phase transitions [30, 31].

3.2 Impact of solution pH on AB14 dye biosorption

An important factor in the adsorption analyses is the pH impact of the medium. Various species may show a different array of appropriate pH depending on the types of biosorbent employed [48, 49]. To establish the optimum pH for the optimization of the sorption process, which is defined by the point at which the surface charge of the sorbent is zero, the point of zero charges is employed (pH_{PZC}). The biosorption of anionic and cationic species is promising when the surface charges on the sorbent are positively and negatively charged owing to the solution pH being less or superior than the pH_{PZC} [38, 50–52]. The pH_{PZC} of MCT was determined to be 9.8 (Fig. 9a). In this study, the impact of the solution pH on the confiscation of AB14 dye using MCT was explored in the array of pH 1.5 to 12 (Fig. 9b). As noticed in Fig. 9, the percentage (%) of AB14 dye confiscated from the biosorbent was drastically decreased with increasing pH values from 1.5 to 12. The optimum % of AB14 dye removed was noticed at pH 1.5 (86.9%). At pH < pH_{PZC}, the surface of the biosorbent was protonated leading to the electrostatic interaction between the positively charged sites on the biosorbent and the anionic AB14 dye, resulting in an increased % of dye removed [53, 54]. With the subsequent increase in the solution pH, a decrease in the % of AB14 dye removed was observed owing to the increasing hydroxyl ions present in the solution and increased negative charge on the biosorbent surface by the deprotonation of the positively charged sites. Hence an electrostatic repulsion between negatively charged sites on the biosorbent surface and negatively charged AB14 dye ions [Aragaw, 2020; Aragaw and Alene, 2022] [55–57].

3.3 Impact of sorbent dosage on AB14 biosorption

To assess the smallest amount necessary for attaining optimum sorption, sorbent dosage optimization is important [22, 58, 59]. The impact of MCT dosage on the % of AB14 dye confiscated is depicted in Fig. 10. The biosorbent dosage

used for this study was varied from 0.25 to 1.25 g/L and at a fixed pH of 1.5. As noticed in Fig. 10a–e, the percentage of AB14 dye confiscated to MCT biosorbent improved with increasing contact time and biosorbent dosage used. This increase in the % of AB14 dye confiscated with enhanced MCT biosorbent dosage was ascribed to the availability of sorption sites on the biosorbent surface, leading to additional prospects for dye ions to stick to the biosorbent. At elevated biosorbent dosage, the percentage of AB14 dye removed remained constant or reached equilibrium, which was attributed to the accumulation of particles sorbed at elevated dosages, the saturation of the pore volume and surface, thereby reducing the surface area accessible for sorption of dye molecules and the intensification in the diffusion path length [60, 61].

3.4 Impact of initial concentration on AB14 dye biosorption

The original dye concentration performs a critical part in the quantity of sorbed dye by the sorbent and the confiscation effectiveness [54]. As noticed in this study, enhancement in the dye concentration from 100 to 400 mg/L led to a decrease in the percentage of confiscation from 84 to 25% with an increase in contact time. This was ascribed to the saturation of the adsorption sites on the adsorbent surface at elevated dye concentrations (Fig. 11) [18]. At low concentrations, the accessible surface area ratio to the initial dye concentration is high and the dye ions diffusion from the solution to the sites on the surface of the biosorbent is enhanced with improved initial concentration, thus enhancing the driving force of the concentration gradient [22, 62].
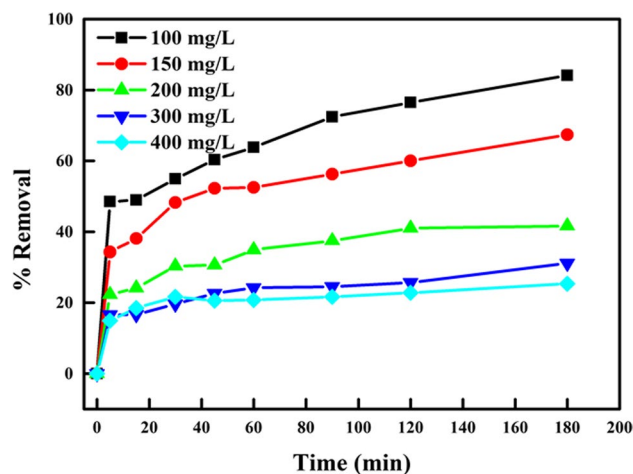

Fig. 11 Impact of initial dye concentration on the biosorption of AB14 dye

3.5 Kinetic models

To study the prospective of employing a solid adsorbent, an adsorption kinetic study is very important, which includes the adsorption rate study to establish the

impacts of different factors on the adsorption processes. This generally arises via a precise careful observation of experimental terms that impacts the rate of the adsorption process, till equilibrium is attained. The data derived from kinetic studies are employed to create necessary
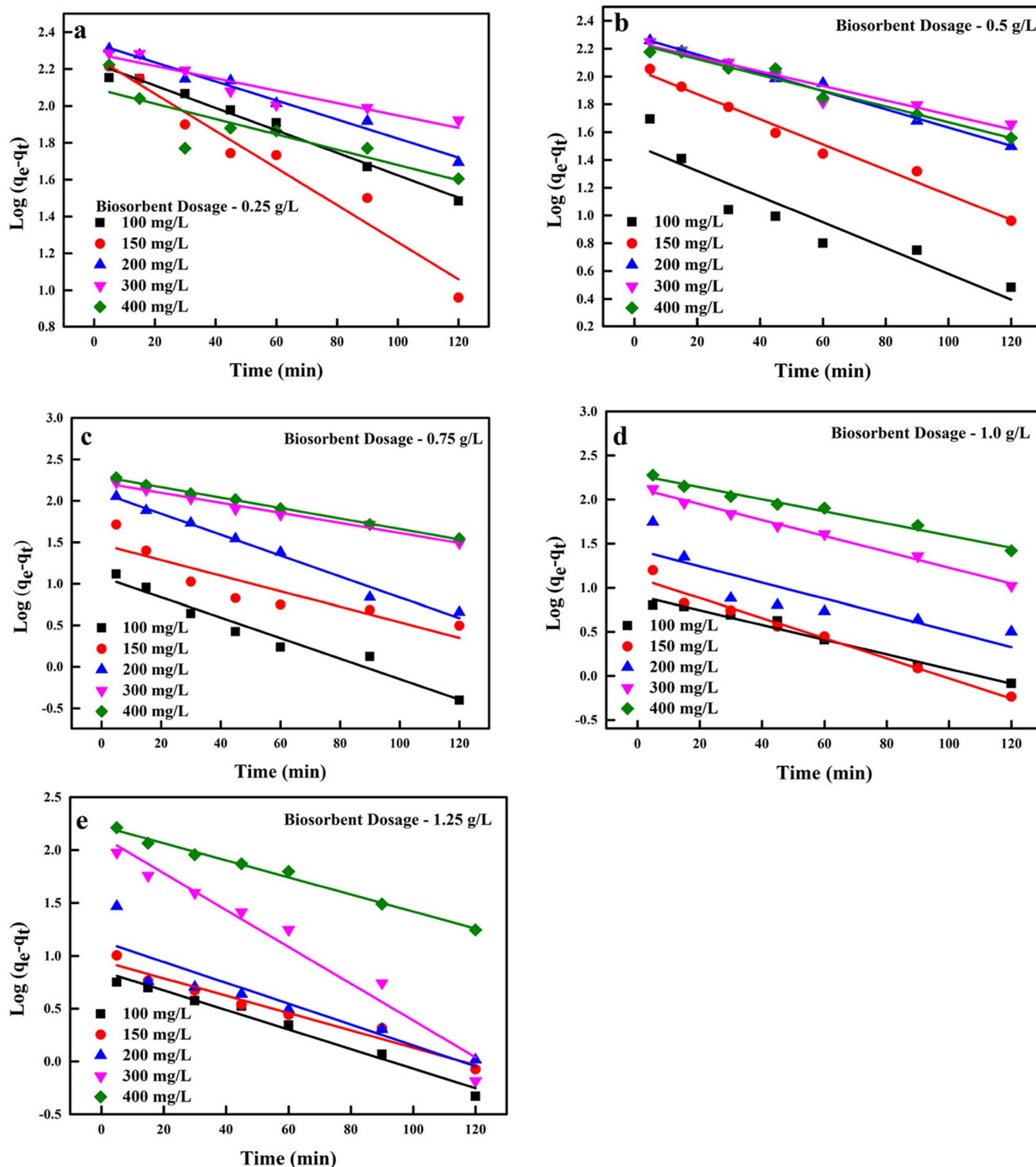

Fig. 12 Linear plot of PFO models at biosorbent dosage of **a** 0.25 g/L, **b** 0.5 g/L, **c** 0.75 g/L, **d** 1.0 g/L, and **e** 1.25 g/L

scientific models to define the adsorbate molecules and solid biosorbent interactions. With unequivocal knowledge of the rate of reaction and the determining factors, suitable biosorbent materials for applications in the industry can be created from these results [63, 64]. The different

kinetic models employed in this study to investigate the complicated dynamics of the biosorption process were the pseudo-first-order (PFO), PSO, intraparticle diffusion (IPD), and film diffusion models (FD) (Fig. 12). A well-known model that is generally employed to highlight the
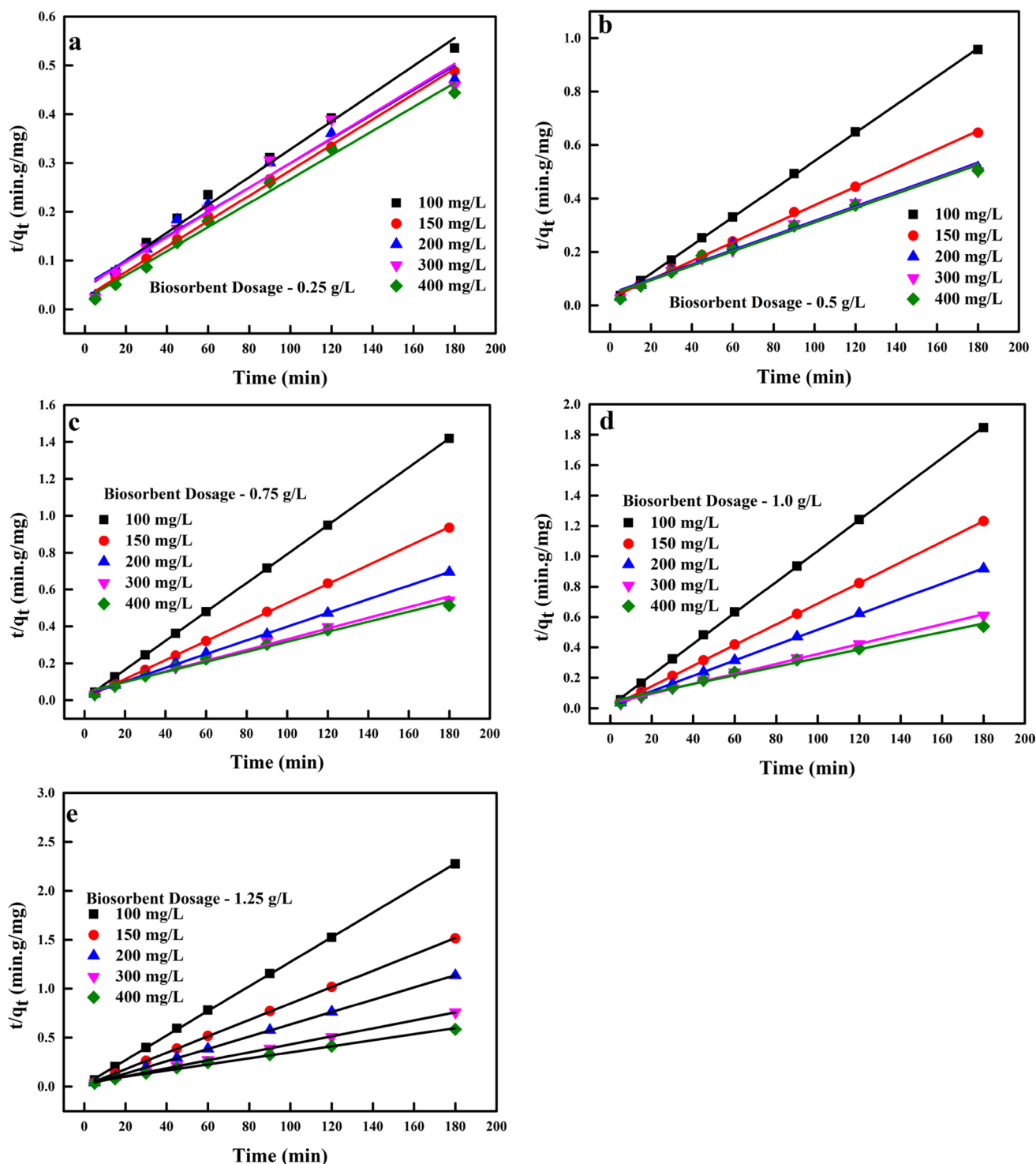
Fig. 13 Linear plot of PSO models at biosorbent dosage of **a** 0.25 g/L, **b** 0.5 g/L, **c** 0.75 g/L, **d** 1.0 g/L, and **e** 1.25 g/L

application of a solid sorbent for the sorption of a sorbate from a water-soluble solution is the Lagergren PFO model. It is presumed in this model that the general rate of adsorption is relative to the variation in the concentrations at saturation and the sum quantity of the solute uptake. It is expressed linearly as Eq. (4) [63–65].
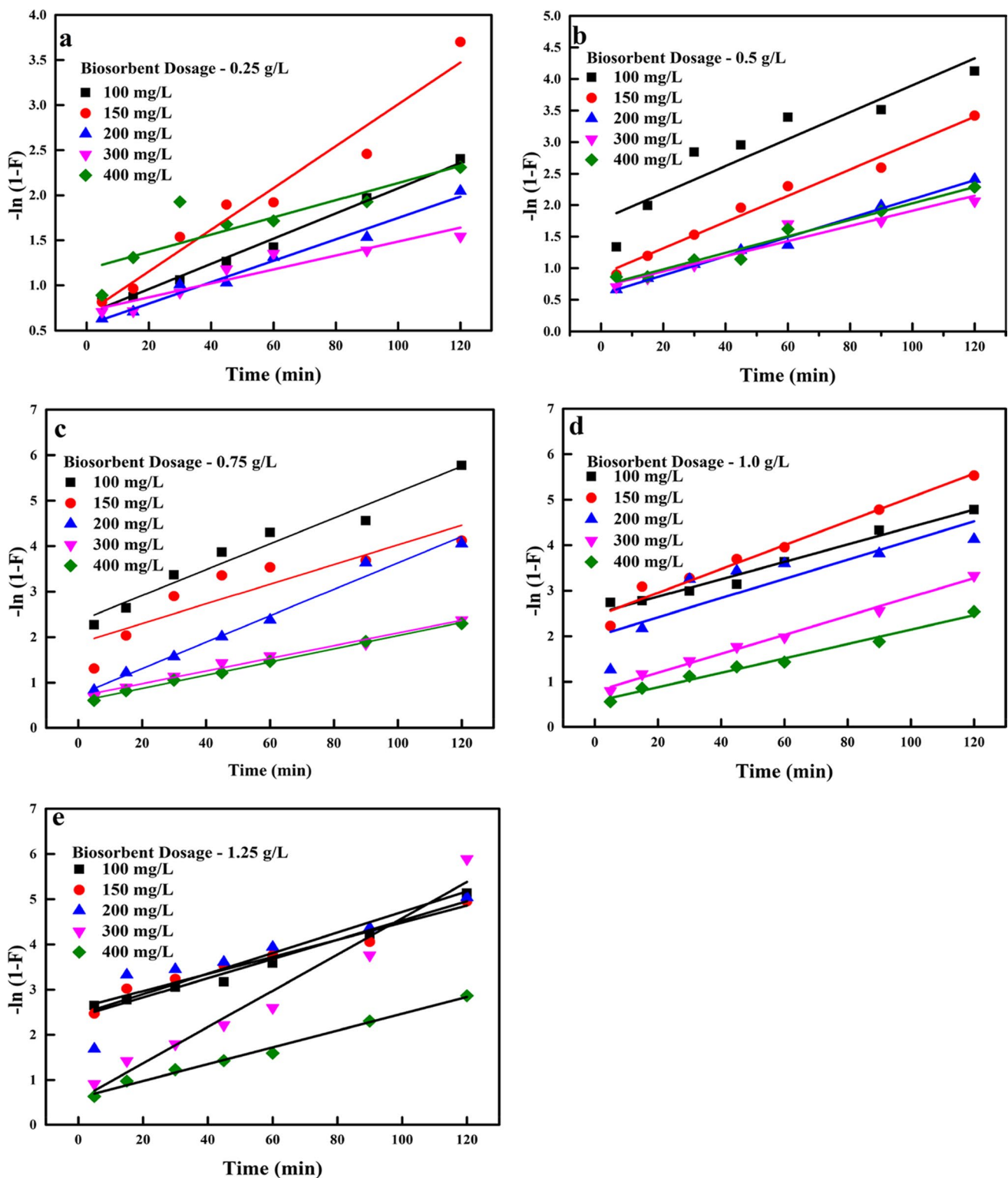
Fig. 14 Linear plots of FD model at biosorbent dosage of **a** 0.25 g/L, **b** 0.5 g/L, **c** 0.75 g/L, **d** 1.0 g/L, and **e** 1.25 g/L

$$Log(q_e - q_t) = Logq_e - \frac{k_1}{2.303}t \qquad (4)$$

k_1 is the PFO rate constant [66]. The linear plot of this model is depicted in Fig. 12 at varying biosorbent dosages.
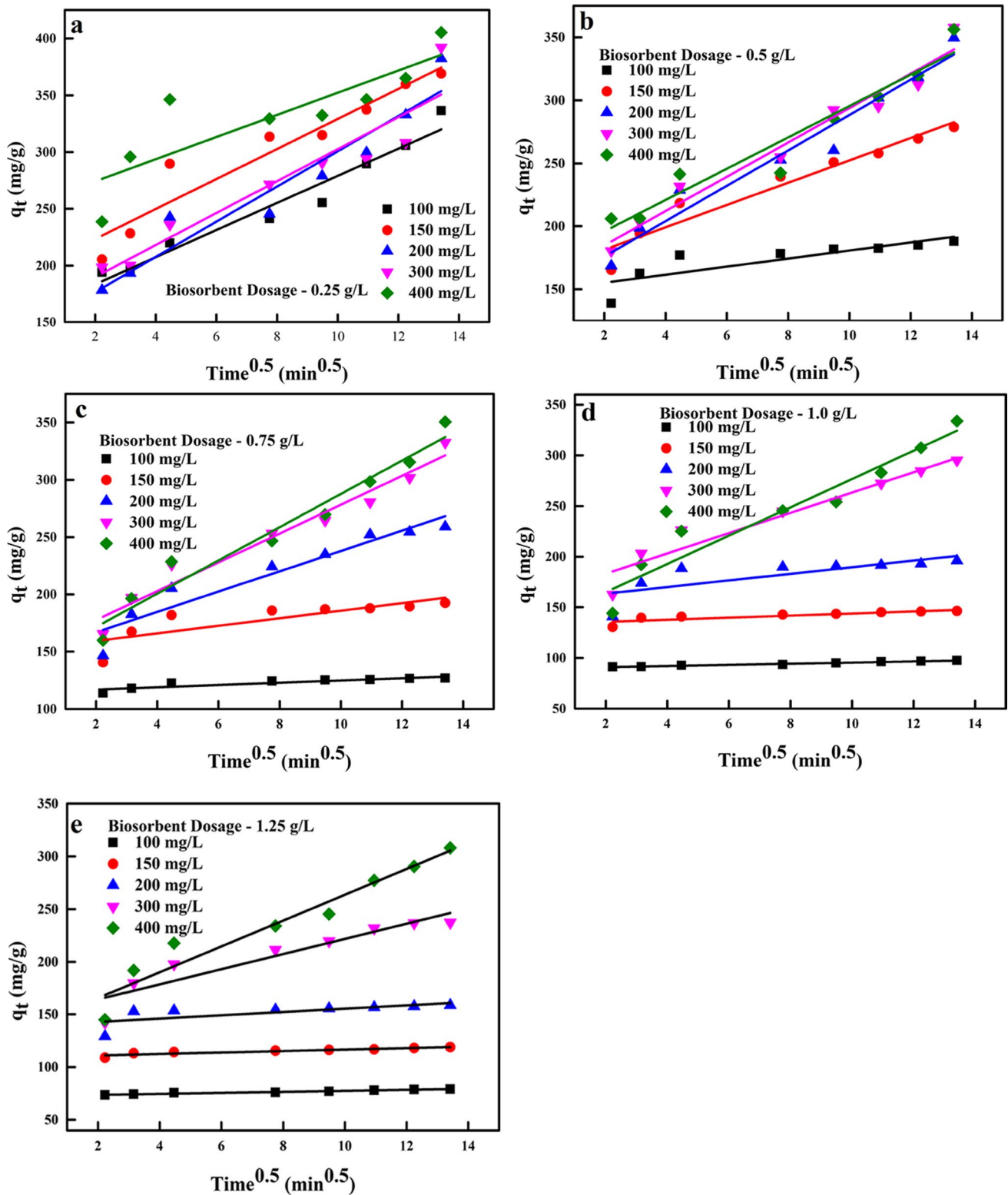
Fig. 15 Linear plots of IPD models at biosorbent dosage of **a** 0.25 g/L, **b** 0.5 g/L, **c** 0.75 g/L, **d** 1.0 g/L, and **e** 1.25 g/L

The PSO rate equation was popularized by Ho and Mckay (1999) [63, 67]. It is employed for evaluating chemisorption kinetics from liquid solutions and defines the sorption of sorbates to biosorbents where the chemical bonding (inter-action) between the sorbates and functional groups on the biosorbent surface are accountable for the sorption capacity of the biosorbent. This is founded on equilibrium sorption, which is reliant on the sorbed sorbate amount to the biosorbent surface and sorbate quantity sorbed at equilibrium. The linearized form of this model and the estimated parameters of this model are represented by Eq. (5) and Fig. 13.

$$\frac{t}{q_t} = \frac{1}{k_2 q_e^2} + \left(\frac{1}{q_e}\right) t \qquad (5)$$

k_2 is the PSO rate constant [68, 69].

The FT model was put forward by Mckay [70–72]. Contaminant transport from the liquid phase to the solid phase is done by mass transfer from one phase to the other. Hence, to know the appropriateness of a sorbent for the process of adsorption, the process effectiveness and effluent treatment plants design, the stages involved in contaminants sorption from water-soluble solution must be known [73]. The FT model presumes that the adsorbate molecules flow via a film of liquid encircling the biosorbent in the rate-controlling stage [74].

The adsorption mechanism of AB14 dye happens in various stages, with the initial stage comprising the AB14 dye moving from the bulk solution to the external surface of the biosorbent. This is followed by AB14 dye diffusion via the boundary layer to the exterior surface of the biosorbent, which involves the biosorption of AB14 dye at active sites on the MCT biosorbent surface. Finally, the intra-particle diffusion and biosorption of AB14 via the MCT particles [75]. Hence, the adsorption mechanism was assessed via the LF and IPT models, and Eq. (6 and 7) defines the LF model.

$$ln(1 - F) = -k_{FD} \times t \qquad (6)$$

Table 1 Determined parameters of the PFO and PSO models

Parameter			PFO model			PSO model		
MCT dosage	AB14 dye Conc. (mg/L)	q_e (exp.)	q_e (calc.)	$k_1 \times 10^3$	R^2	q_e (calc.)	$k_2 \times 10^3$	R^2
0.25 g L^{-1}	100	336.33	0.346	14.05	0.986	357.14	0.18	0.988
	150	368.97	0.356	23.26	0.959	384.62	0.27	0.998
	200	382.19	0.369	11.98	0.981	400.00	0.13	0.977
	300	392.00	0.359	7.83	0.896	400.00	0.14	0.965
	400	405.32	0.321	9.67	0.730	400.00	0.30	0.991
0.5 g L^{-1}	100	188.06	0.178	21.42	0.865	188.68	2.10	1.000
	150	278.70	0.313	20.96	0.982	285.71	0.46	0.999
	200	349.44	0.360	15.20	0.992	370.37	0.17	0.989
	300	357.74	0.351	11.98	0.942	370.37	0.18	0.987
	400	356.21	0.350	13.13	0.972	370.37	0.18	0.987
0.75 g L^{-1}	100	126.94	0.356	28.33	0.961	128.21	7.07	1.000
	150	192.51	0.169	21.65	0.807	192.31	2.31	1.000
	200	259.02	0.322	29.02	0.986	270.27	0.51	0.999
	300	332.59	0.346	13.82	0.985	344.83	0.21	0.991
	400	350.45	0.360	14.51	0.996	370.37	0.16	0.989
1.0 g L^{-1}	100	97.54	-0.041	19.11	0.978	98.04	7.13	1.000
	150	146.25	0.046	26.25	0.973	147.06	6.25	1.000
	200	196.02	0.154	21.19	0.737	196.08	2.53	1.000
	300	295.09	0.328	20.73	0.993	303.03	0.37	0.998
	400	333.88	0.358	15.89	0.983	22.22	31.64	0.991
1.25 g L^{-1}	100	79.16	-0.067	21.19	0.977	79.37	8.77	1.000
	150	118.88	-0.022	18.88	0.961	119.05	7.06	1.000
	200	158.50	0.057	22.80	0.813	158.73	5.29	1.000
	300	237.29	0.053	40.07	0.960	243.90	0.72	1.000
	400	308.02	0.348	18.65	0.991	322.58	0.24	0.995

$$F = \frac{q_t}{q_e} \tag{7}$$

F and k_{FD} represent fractional attainment of equilibrium, and film diffusion rate coefficient (L/min). A plot of ln (1-F) against t, with a zero intercept, indicates that the sorption process kinetics are regulated by the diffusion via the liquid film around the biosorbent [64]. As observed in Fig. 14, the experimental data of the biosorption of AB14 dye adsorption to the MCT biosorbent at various initial concentrations (100–400 mg/L) of AB14 dye did not provide a straight line that goes via the origin and the coefficient of regression were in the range of 0.730–0.998 (Table 3). This was indicative of the dye diffusion in the liquid film all around the MCT biosorbent was not a rate-defining phase but may promote the biosorption process mostly at the biosorption process start [74, 76, 77].

In this study, the IPD model proposed by Weber and Morris was used to explore the likelihood of IPD resistance [63, 78]. The IPD model splits the sorption process into the movement of solutes molecules from water-soluble solution to the biosorbent particle surface and the sorbate molecule diffusion into the biosorbent inner pores. The linear form of this model is expressed as Eq. (8):

$$q_t = k_{dif}t^{0.5} + C \tag{8}$$

k_{dif} and C (mg·g^{-1}·min$^{-0.5}$) are the IPD model rate constant and the IPD constants relating to boundary layer thickness (mg·g^{-1}), which are determined from the slope and intercept of the graph of q_t against the square root of time (t$^{0.5}$). This model undertakes that if the plot takes a straight line cutting the origin, then the sorption process is operated by pore diffusion and the solute ions diffuse within the biosorbent material capillaries and pores. As observed in the linear plot of this model at varying biosorbent dosage (Fig. 15), the fitting to experimental data using this model did not maintain linearity, which was indicative of the process not only being controlled by rate-limiting diffusion but by other adsorption processes [79, 80]. From the determined parameters obtained from the fitting of the models to the experimental data in Tables 1 and 2, it was noticed that the PSO model when compared to other models best define the adsorption process of AB14 dye to MCT biosorbent with a coefficient of regression (R^2) > 0.98, which were close to unity. Thus, based on the unsurpassed fitting of this model, chemisorption was a rate-limiting stage of the sorption process of AB14 dye.

Table 2 Calculated parameters of IPD and FD models

MCT dosage	AB14 dye Conc (mg/L)	IPD model			FD model	
		K_{dif}	C	R^2	K_{FD}	R^2
0.25 g L^{-1}	100	11.95	159.55	0.958	− 0.01	0.986
	150	13.23	196.89	0.918	− 0.02	0.959
	200	15.51	145.57	0.926	− 0.01	0.981
	300	14.08	161.75	0.892	− 0.01	0.896
	400	9.75	254.71	0.718	− 0.01	0.730
0.5 g L^{-1}	100	3.19	148.77	0.700	− 0.02	0.865
	150	8.87	163.66	0.940	− 0.02	0.982
	200	14.05	147.79	0.958	− 0.02	0.992
	300	13.63	157.48	0.963	− 0.01	0.942
	400	12.44	171.08	0.939	− 0.01	0.972
0.75 g L^{-1}	100	0.99	114.98	0.823	− 0.03	0.961
	150	3.29	152.82	0.663	− 0.02	0.808
	200	8.88	149.17	0.911	− 0.03	0.986
	300	12.59	152.45	0.960	− 0.01	0.985
	400	14.52	142.55	0.960	− 0.01	0.998
1.0 g L^{-1}	100	0.57	89.75	0.977	− 0.02	0.978
	150	1.04	133.47	0.747	− 0.03	0.973
	200	3.27	156.80	0.582	− 0.02	0.737
	300	10.01	163.20	0.929	− 0.02	0.993
	400	13.97	136.92	0.935	− 0.02	0.983
1.25 g L^{-1}	100	0.48	72.66	0.973	− 0.02	0.977
	150	0.70	109.60	0.863	− 0.02	0.961
	200	1.56	139.72	0.491	− 0.02	0.813
	300	7.19	149.85	0.870	− 0.04	0.960
	400	12.25	141.09	0.935	− 0.02	0.991
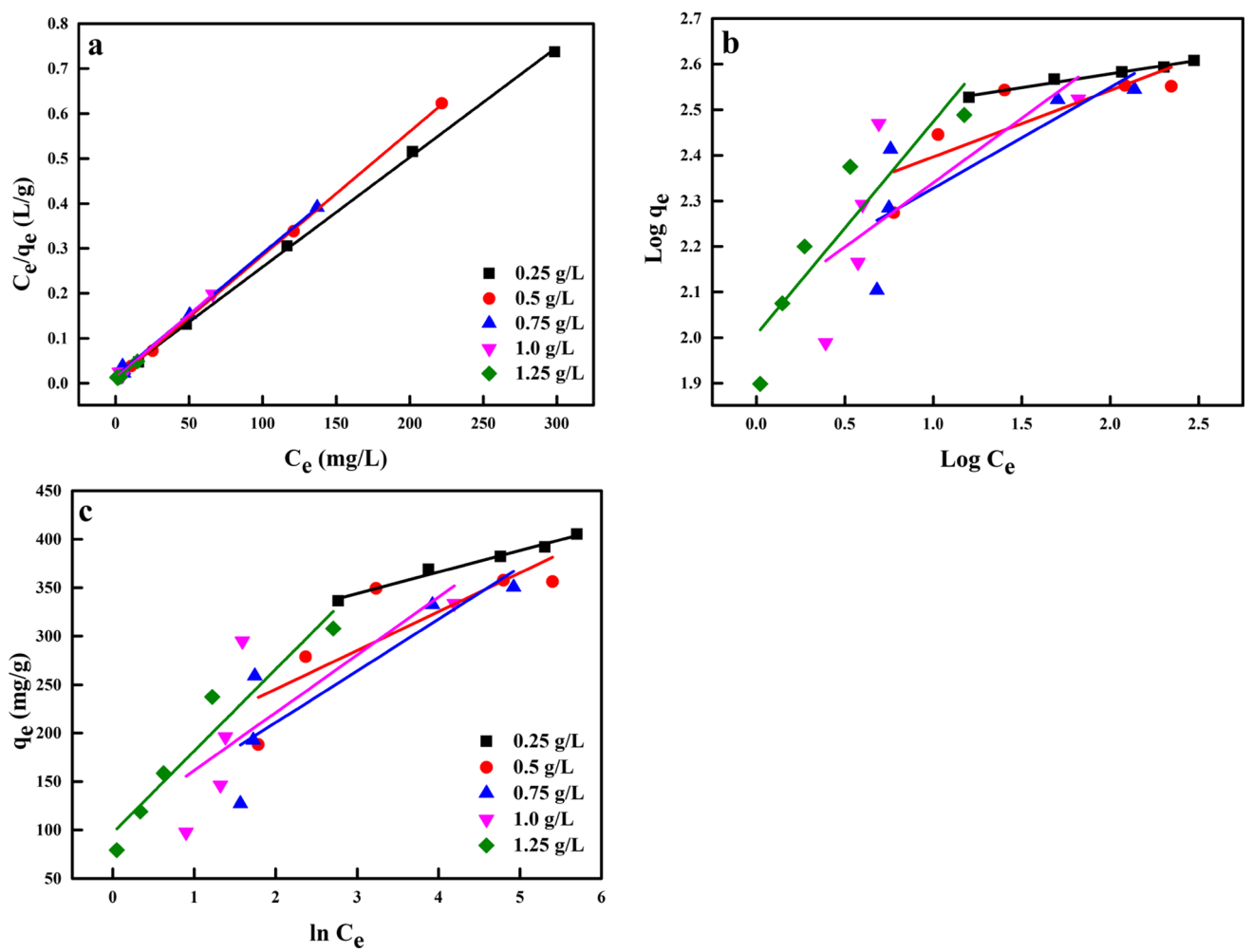
Fig. 16 Linear plots of **a** LNR model, **b** FRH model, and **c** TMN models

3.6 Isotherm models

To comprehend the process and sorbate distribution between the liquid and solid biosorbent stage at equilibrium during the removal process, the adsorption isotherms are employed [63, 81]. The Freundlich (FRH) model is an empirical model that is generally employed to explain diverse systems such as sorption of natural compounds or extremely interactive species to

nanomaterials. The linear form of this model is expressed as Eq. (6). While the Langmuir (LNR) model defines consistent sorption, where an individual molecule retains continuous enthalpy and sorption activation energy (individual sites acquiring the same attraction for the sorbate), with no drifting of the sorbate within the sorbent surface and the sorbate molecules creating a monolayer on the surface of the sorbent [82]. This model is effective for monolayer biosorption on a surface

Table 3 Obtained parameters of LNR and FRH Models

Isotherm	Parameters	MCT dosage				
Models		0.25 g/L	0.5 g/L	0.75 g/L	1.0 g/L	1.25 g/L
Linear LNR	Q_m	416.67	357.14	370.37	357.14	370.37
	$b \times 10^3$	171.43	329.41	183.67	245.61	350.65
	R^2	0.99	0.99	1.00	0.99	0.98
FRH	$1/n$	16.67	6.86	4.52	3.54	2.14
	K_F	11.69	9.50	8.22	7.83	7.44
	R^2	0.98	0.664	0.66	0.54	0.83

Table 4 Comparison of the maximum adsorption capacities (q_m) of AB14 dye using different adsorbents

Adsorbents	q_m	References
MCT	416.67 mg/g	This study
Calcined Mg/Fe layered double hydroxide (CLDH)	370.00 mg/g	[88]
Mg/Fe layered double hydroxide (LDH)	41.70 mg/g	
Magnetic carbon nano-composite	20.5 mg/g	[89]
Brown sea bean (*Mucuna Sloanei*) shell	500.00 mg/g	[90]
Granular activated carbon	27.45 mg/g	[91]
Macronet resin (Macronet MN200 and MN300)	64.52 mg/g and 107.50 mg/g	[92]

comprising of a fixed number of similar sites and even sorption [83, 84]. The linearized forms of these models are defined by Eqs. (9) and (10).

$$Log q_e = Log K_F + \frac{1}{n} Log C_e \qquad (9)$$

$$\frac{C_e}{q_e} = \frac{C_e}{Q_m} + \frac{1}{Q_m b} \qquad (10)$$

K_F and n, Q_m, and b are the FRH model constants that are indicative of the intensity and sorption capacity, the maximum quantity of biosorption capacity, and the energy of sorption LNR constant [9, 66]. The TMN model studies the biosorbent and pollutant interaction as a chemical adsorption process [75, 85, 86]. It is assumed in this model that the adsorption is described by the homogeneous distribution of the binding energies. Its linear form is described by Eq. (11) [87].

$$q_e = B \ln(A_T) + B \ln(C_e) \qquad (11)$$

The graph of q_e against $\ln C_e$ allows for the determination of TMN constants A_T and B, which are the equilibrium binding and sorption heat constants ($B = RT/b$, R, T and b are the universal gas constant, absolute temperature and TMN isotherm constants) [78]. The linearized plot of the various models is depicted in Fig. 16. All the parameters determined from fittings using various isotherm models are tabulated in Table 3. The determined R^2 for the LNR model were much higher than those for the FRH model, which was indicative of the adsorption of AB14 dye by MCT biosorbent being described by the LNR model owing to the equal and homogeneous spread of the dye molecules over the porous surface of the biosorbent. The optimum adsorption capacity is assessed to be 416.67 mg/g and the adsorption process was suggestive of monolayer sorption of AB14 dye to MCT biosorbent. From the literature reviewed and which are summarized in Table 4, the effectiveness of the removal of AB14 dye using different adsorbents was compared with the MCT adsorbent and it was noticed that MCT adsorbent was more effective in removing AB14 dye in comparison to other adsorbents employed in the confiscation of AB14 dye.

3.7 Regeneration of activated biomass–based biosorbent

According to a recent review study by Aragaw and Bogale [35], several studies have shown that the regeneration procedures such as thermal, microwave irradiation, wet air oxidation, microbial/biological, chemical/solvent regenerations, etc. are cost-effective and have possible low energy consumption. The chemical/solvent regeneration has been reported to be more extensively used with the adsorbents having multiple effective adsorption–desorption cycles, where NaCl and HCl were reported to be among the best activating agents that had better performance throughout the desorption process [35]. Hence, the desorption experiments of AB14 dye from the loaded MCT were performed using 0.1 M NaOH followed by 0.1 N HCl as eluted mediums to investigate the economic feasibility and reusability of MCT as an adsorbent. In this condition. The desorption % decreased with rising regeneration cycles Fig. 17. The regenerated MCT was applied in six consecutive cycles of adsorption/desorption. The adsorption amount presented was consistent through the cycles and experienced the adsorption capacity decreased by 12.7% after
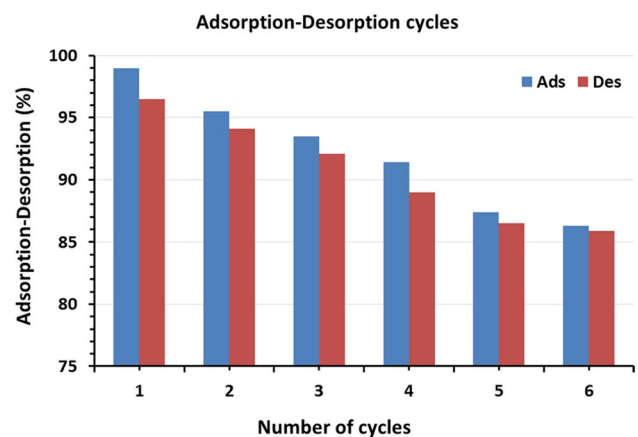
Fig. 17 Desorption % of AB14 dye from MCT using 0.1 M NaOH and 0.1 N HCl and the adsorption cycles of AB14 dye by regenerated MCT

six generations, which suggests it may be used as a sustainable AB14 dye removal (Fig. 17).

4 Conclusion

In this study, the prospect of using an MCT biosorbent synthesized from mandarin peels for the removal of AB14 dye was investigated. The synthesized MCT biosorbent was characterized using FTIR, TGA, BET, and SEM together with an EDX. The biosorption of the AB14 dye using MCT biosorbent was observed to be pH-dependent, where the optimum removal of the AB14 dye was noticed at pH 1.5 and was attributed to the electrostatic interaction between the biosorbent positively charged sites and the anionic AB14 dye. Also, the biosorption process of AB14 dye using MCT biosorbent was ideally described, employing the PSO and the LNR models. The determined adsorption capacity was estimated to be 416.67 mg/g and the adsorption process was indicative of monolayer sorption of AB14 dye to MCT biosorbent. The study has further revealed that biosorbents prepared from low-cost agronomic waste materials such as MCT biosorbent can efficiently be beneficial for the removal of dyes and other effluents from industrial toxic wastes before they are further released into the environment. Hence, it is recommended that more research on the application of low-cost agronomic waste materials such as biosorbents for the mitigation of environmental effluences vis-à-vis industrial toxic wastes management should be strengthened.

Data availability Data sharing does not apply to this article.

Declarations

Consent to participate Not applicable.

Conflict of interest The authors declare no competing interests.

References

1. El Nemr A (2011) Impact, monitoring and management of environmental pollution. Nova Science Publishers, Inc. Hauppauge New York. [ISBN-10: 1608764877, ISBN-13: 9781608764877]. 638 pages.

2. El Nemr A (2012) Environmental pollution and its relation to climate change. Nova Science Publishers, Inc. Hauppauge New York. [ISBN-13: 978–1–61761–794–2]. 694 pages.

3. Kerry RG, Ukhurebor KE, Kumari S, Maurya GK, Patra S, Panigrahi B, Majhi S, Rout JR, Rodriguez-Torres MDP, Das G, Shin H-S, Patra JK (2021) A comprehensive review on the applications of nano-biosensor based approaches for non-communicable and communicable disease detection. Biomater Sci 9:3576–3602. https://doi.org/10.1039/d0bm02164d

4. Ukhurebor KE, Aidonojie PA (2021) The influence of climate change on food innovation technology: review on topical developments and legal framework. Agriculture & Food Security 10:1–14. https://doi.org/10.1186/s40066-021-00327-4

5. Ukhurebor KE, Singh KRB, Nayak V, UK-Eghonghon G (2021) Influence of SARS-CoV-2 pandemic: a review from the climate change perspective. Environ Sci: Process Imp 23:1060–1078. https://doi.org/10.1039/d1em00154j

6. Onyancha RB, Ukhurebor KE, Aigbe UO, Osibote OA, Kusuma HS, Darmokoesoemo H, Balogun VA (2021) A Systematic review on the detection and monitoring of toxic gases using carbon nanotube-based biosensors. Sensing and Bio-Sensing Res 34:100463. https://doi.org/10.1016/j.sbsr.2021.100463

7. El Nemr A (2012) Textiles: types, uses and production methods. Nova Science Publishers, Inc. Hauppauge New York. Hard cover [ISBN: 978–1–62100–239–0], e-book [ISBN: 978–1–62100–284–0]. 621 pages.

8. Akpomie KG, Conradie J (2021) Ultrasonic-assisted adsorption of eriochrome black T and celestine blue dyes onto *Ipomoea batatas*-derived biochar. Inter J Environ Analyt Chem 1-19 https://doi.org/10.1080/03067319.2021.1995724

9. Aigbe UO, Ukhurebor KE, Onyancha RB, Osibote OA, Darmokoesoemo H, Kusuma HS (2021) Fly ash-based adsorbent for adsorption of heavy metals and dyes from aqueous solution: a review. J Mater Res Technol 14:2751–2774. https://doi.org/10.1016/j.jmrt.2021.07.140

10. Ibrahima E, Moustafab H, El-molla SA, Halim SD, Ibrahim SS (2021) Integrated experimental and theoretical insights for malachite green dye adsorption from wastewater using low-cost adsorbent. Water Sci Technol 84:3833–3858. https://doi.org/10.2166/wst.2021.489

11. Ukhurebor KE, Aigbe UO, Onyancha RB, Nwankwo W, Osibote OA, Paumo HK, Ama OM, Adetunji CO, Siloko IU (2021) Effect of hexavalent chromium on the environment and removal techniques: a review. J Environ Managem 280:111809. https://doi.org/10.1016/j.jenvman.2020.111809

12. Onyancha RB, Aigbe UO, Ukhurebor KE, Muchiri PW (2021) Facile synthesis and applications of carbon nanotubes in heavy-metal remediation and biomedical fields: a comprehensive review. J Mol Struct 1238:130462. https://doi.org/10.1016/j.molstruc.2021.130462

13. Sudarni DHA, Aigbe UO, Ukhurebor KE, Onyancha RB, Kusuma HS, Darmokoesoemo H, Osibote OA, Balogun VA, Widyaningrum BA (2021) Malachite green removal by activated potassium hydroxide clove leaves agro-waste biosorbent: characterization,

kinetics, isotherms and thermodynamics studies. Adsorpt Sci Technol 1145312:1–15. https://doi.org/10.1155/2021/1145312

14. Ukhurebor KE, Onyancha RB, Aigbe UO, UK-Eghonghon G, Kerry RG, Kusuma HS, Darmokoesoemo H, Osibote OA, Balogun VA (2022) A methodical review on the applications and potentialities of using nanobiosensors for diseases diagnosis. Biomed Res Int 1682502:1–20. https://doi.org/10.1155/2022/1682502

15. El Nemr A, Ragab S (2018) Acetylation of Cotton-Giza 86 cellulose using $MnCl_2$ as a new catalyst and its application to machine oil removal. Environ Process 5:895–905. https://doi.org/10.1007/s40710-018-0330-7

16. Ukhurebor KE, Athar H, Adetunji CO, Aigbe UO, Onyancha RB, Abifarin O (2021) Environmental implications of petroleum spillages in the Niger Delta region of Nigeria: A review. J Environ Managem 293:112872. https://doi.org/10.1016/j.jenvman.2021.112872

17. Parsa BJ, Vahidian RH, Soleymani AR, Abbasi M (2011) Removal of Acid Brown 14 in aqueous media by electrocoagulation: optimization parameters and minimizing of energy consumption. Desalination 278:295–302. https://doi.org/10.1016/j.desal.2011.05.040

18. Hasanzadeh M, Jorfi S, Ahmadi M, Jaafarzadeh N (2020) Hybrid sono-photocatalytic degradation of Acid Brown 14 using persulphate and ZnO nanoparticles: feasibility and kinetic study. Inter J Environ Analyt Chem 1-14 https://doi.org/10.1080/03067319.2020.1790543

19. Helmy ET, El Nemr A, Mousa M, Arafa E, Eldafrawy S (2018) Photocatalytic degradation of organic dyes pollutants in the industrial textile wastewater by using synthesized TiO_2, C-doped TiO_2, S-doped TiO_2 and C, S co-doped Ti_O2 nanoparticles. J Water Environ Nanotech 3:116–127

20. Ama O, Wilson A, Ray S (2018) Photoelectrochemical degradation of methylene blue dye under visible light irradiation using EG/Ag-ZrO_2 nanocomposite electrodes. Inter J Electrochem Sci 14:9982–10001. https://doi.org/10.1016/s1001-0742(10)60489-5

21. El Nemr A, Helmy ET, Arafa E, Eldafrawy S, Mousa M (2019) Photocatalytic and biological activities of undoped and doped TiO_2 prepared by Green method for water treatment. J Environ Chem Eng 7:103385. https://doi.org/10.1016/j.jece.2019.103385

22. Aigbe U, Das R, Ho W, Srinivasu V, Maity A (2018) A novel method for removal of Cr (VI) using polypyrrole magnetic nanocomposite in the presence of unsteady magnetic fields. Sep Purif Technol 194:377–387. https://doi.org/10.1016/j.seppur.2017.11.057

23. Mohanan, N., Montazer, Z., Sharma, P., Levin, D. (2020). Microbial and enzymatic degradation of synthetic plastics. Frontiers in Microbiology, 11. https://doi.org/10.3389/2Ffmicb.2020.580709

24. Hassaan MA, El Nemr A, Madkour FF (2017) Testing the advanced oxidation processes on the degradation of direct blue 86 dye in wastewater. Egypt J Aquat Res 43:11–19. https://doi.org/10.1016/j.ejar.2016.09.006

25. Hassaan MA, El Nemr A, Madkour FF (2017) Advanced oxidation processes of mordant Violet 40 dye in freshwater and seawater. Egypt J Aquat Res 43:1–9. https://doi.org/10.1016/j.ejar.2016.09.004

26. El Nemr, M.A. Hassaan, F.F. Madkour, A.M. Idris, T.O. Said, T. Sahlabji, M.M. Alghamdi, A.A. El-Zahhar (2021). Advanced oxidation of AY-11 dye effluent: detoxification and Degradat Mechanism Toxin Rev 40:1472–1480. https://doi.org/10.1080/15569543.2020.1736098

27. Hassaan MA, El Nemr A, Ragab S (2021) Green synthesis and application of metal and metal oxide nanoparticles. Handbook of Nanomaterials and Nanocomposites for Energy and

Environmental Applications. Book chapter. Springer Chapter 36:831–857. https://doi.org/10.1007/978-3-030-11155-7_125-1

28. Hassaan MA, Elkatory MR, El Nemr A (2021) Applications of photochemical oxidation in Textile Industry. Handbook of Nanomaterials and Nanocomposites for Energy and Environmental Applications. Book chapter. Springer Chapter 86:1975–2003. https://doi.org/10.1007/978-3-030-36268-3_59

29. El Nemr A (2012) Non-Conventional textile waste water treatment. Nova Science Publishers, Inc. Hauppauge New York. [Hard cover ISBN: 978–1–62100–079–2, e-book ISBN: 978–1–62100–228–4] 267 pages.

30. El-Nemr MA, Ismail IMA, Abdelmonem NM, Ragab S, El Nemr A (2020) Ozone and ammonium hydroxide modification of biochar prepared from pisum sativum peels improves the adsorption of copper (II) from an aqueous medium. Environ Process 7:973–1007. https://doi.org/10.1007/s40710-020-00455-2

31. El-Nemr MA, Abdelmonem NM, Ismail IMA, Ragab S, El Nemr A (2020) The efficient removal of the hazardous azo dye acid orange 7 from water using modified biochar from pea peels. Desal Water Treatment 203:327–355. https://doi.org/10.5004/dwt.2020.26190

32. El-Nemr MA, Abdelmonem NM, Ismail IMA, Ragab S, El Nemr A (2020) Removal of acid yellow 11 dye using novel modified biochar derived from watermelon peels. Desal Water Treatment 203:403–431. https://doi.org/10.5004/dwt.2020.26207

33. El-Nemr MA, Ismail IMA, Abdelmonem NM, El Nemr A, Ragab S (2021) Amination of biochar derived from watermelon peel by triethylenetetramine and ammonium hydroxide for toxic chromium removal enhancement. Chinese J Chem Eng 36:199–222. S1004-9541(20)30464-X

34. Sahlabji T, El-Nemr MA, El Nemr A, Ragab S, Alghamdi MM, El-Zahhar AA, Idris AM, Said TO (2021) High surface area microporous activated carbon from pisum sativum peels for hexavalent chromium removal from aquatic environment. Toxin Rev In Press. https://doi.org/10.1080/15569543.2021.1908361

35. Aragaw TA, Bogale FM (2021) Biomass-based adsorbents for removal of dyes from wastewater: a review. Front Environ Sci 9:1–24. https://doi.org/10.3389/fenvs.2021.764958

36. Aigbe UO, Ukhurebor KE, Onyancha RB, Okundaye B, Pal K, Osibote OA, Esiekpe EL, Kusuma HS, Darmokoesoemo H (2022) A facile review on the sorption of heavy metals and dyes using bionanocomposites. Adsorp Sci Tech 8030175:1–36. https://doi.org/10.1155/2022/8030175

37. Ayalew AA, Aragaw TA (2020) Utilization of treated coffee husk as low-cost bio-sorbent for adsorption of methylene blue. Adsorp Sci Tech 38:205–222. https://doi.org/10.1177/0263617420920516

38. Aigbe UO, Osibote OA (2021) Carbon derived nanomaterials for the sorption of heavy metals from aqueous solution: a review. Environ Nanotech Monitor Managem 100578 https://doi.org/10.1016/j.enmm.2021.100578

39. Duan C, Ma T, Wang J, Zhou Y (2020) Removal of heavy metals from aqueous solution using carbon-based adsorbents: a review. J Water Process Eng 37:101339. https://doi.org/10.1016/j.jwpe.2020.101339

40. El Nemr A, El-Assal AA, El Sikaily A, Mahmoud ME, Amira MF, Ragab S (2021) New magnetic cellulose nanobiocomposites for Cu(II), Cd(II) and Pb(II) ions removal: Kinetics, thermodynamics and analytical evaluation. Nanotech Environ Eng 6:1–20. https://doi.org/10.1007/s41204-021-00138-9

41. El-Nemr MA, Aigbe UO, Hassaan MA, Ukhurebor KE, Ragab S, Onyancha RB, Osibote OA, El Nemr A (2022) The use of biochar-NH_2 produced from watermelon peels as a natural adsorbent for the removal of Cu(II) ion from water. Biomass Conversion and Biorefinery, In press. https://doi.org/10.1007/s13399-022-02327-1

42. Morton JF (1987) Mandarin orange. Fruits of warm climates. Purdue University, New Crop Resource Online Program. Center for New Crops and Plant Products, pp 142–145

43. Tran HN, Huang F-C, Lee C-K, Huan-Ping Chao H-P (2017) Activated carbon derived from spherical hydrochar functionalized with triethylenetetramine: synthesis, characterizations, and adsorption application. Green Process Synth 6:565–576. https://doi.org/10.1515/gps-2016-0178/html

44. Gregg SJ, Sing KSW (1982) Adsorption surface area and porosity, 2nd edn. Academic Press INC., London

45. Rouquerol F, Rouquerol J, Sing KSW (1999) Adsorption by powders and porous solids. Academic Press INC., London

46. Barrett EP, Joyner LG, Halenda PP (1951) The determination of pore volume and area distributions in porous substances. I. computations from nitrogen isotherms. J Amer Chem Soc 73:373–380. https://doi.org/10.1021/JA01151A046

47. Aragaw TA, Angerasa FT (2020) Synthesis and characterization of Ethiopian kaolin for the removal of basic yellow (BY 28) dye from aqueous solution as a potential adsorbent. Heliyon 6:e04975. https://doi.org/10.1016/j.heliyon.2020.e04975

48. Cardoso NF, Lima EC, Pinto IS, Amavisca CV, Royer B, Pinto RB, Alencar WS, Pereira SF (2011) Application of cupuassu shell as biosorbent for the removal of textile dyes from aqueous solution. J Environ Managem 92:1237–1247. https://doi.org/10.1016/j.jenvman.2010.12.010

49. Eldeeb TM, El Nemr A, Khedr MH, El-Dek SI (2021) Novel bio-nanocomposite for efficient copper removal. Egypt J Aquat Res 47:261–267. https://doi.org/10.1016/j.ejar.2021.07.002

50. Aigbe UO, Osibote OA (2020) A review of hexavalent chromium removal from aqueous solutions by sorption technique using nano-materials. J Environ Chem Eng 104503https://doi.org/10.1016/j.jece.2020.104503

51. Eldeeb TM, El Nemr A, Khedr MH, El-Dek SI, Imam NG (2021) Efficient removal of Cu(II) from water solution using magnetic chitosan nanocomposite. Nanotechnology for Environ Eng 6:34. https://doi.org/10.1007/s41204-021-00129-w

52. El Nemr A, Aboughaly RM, El Sikaily A, Ragab S, Masoud MS (2021) Ramadan MS (2021) Utilization of sugarcane bagasse/ZnCl₂ for sustainable production of microporous nano activated carbons of type I for toxic Cr(VI) removal from aqueous environment. Biomass Conver Bioref In press 10:03. https://doi.org/10.1007/s13399-021-01445-6

53. Aigbe UO, Khenfouch M, Ho W, Maity A, Vallabhapurapu VS, Hemmaragala NM (2018) Congo red dye removal under the influence of rotating magnetic field by polypyrrole magnetic nanocomposite. Desal Water Treat 131:328–342. https://doi.org/10.5004/dwt.2018.23028

54. Namjoufar M, Farzi A, Karimi A (2021) Removal of Acid Brown 354 from wastewater by aminized cellulose acetate nanofibers: experimental and theoretical study of the effect of different parameters on adsorption efficiency. Water Sci Technol 83:1649–1661. https://doi.org/10.2166/wst.2021.070

55. Qin P, Yang Y, Zhang X, Niu J, Yang H, Tian S, Zhu J, Lu M (2018) Highly efficient, rapid, and simultaneous removal of cationic dyes from aqueous solution using monodispersed mesoporous silica nanoparticles as the adsorbent. Nanomaterials 8:4. https://doi.org/10.3390/nano8010004

56. Aragaw TA (2020) Recovery of iron hydroxides from electro-coagulated sludge for adsorption removals of dye wastewater: adsorption capacity and adsorbent characteristics. Surfaces and Interfaces 18:100439. https://doi.org/10.1016/j.surfin.2020.100439

57. Aragaw TA, Alene AN (2022) A comparative study of acidic, basic, and reactive dyes adsorption from aqueous solution onto kaolin adsorbent: Effect of operating parameters, isotherms,

58. kinetics, and thermodynamics. Emerging Contaminants 8:59–74. https://doi.org/10.1016/j.emcon.2022.01.002

58. El Nemr A, Shoaib AGM, El Sikaily A, Ragab S (2021) Mohamed AE-DA, Hassan AF (2021) Utilization of green alga *Ulva lactuca* for sustainable production of meso-micro porous nano activated carbon for adsorption of Direct Red 23 dye from aquatic environment. Carbon Letters In press 02:06. https://doi.org/10.1007/s42823-021-00262-1

59. El Nemr A, Aboughaly RM, El Sikaily A, Masoud MS, Ramadan MS, Ragab S (2021) Microporous activated carbons with a high surface area of type I adsorption isotherm derived from sugarcane bagasse impregnated with zinc chloride. In press, Carbon Letter. https://doi.org/10.1007/s42823-021-00270-1

60. Aigbe UO, Onyancha RB, Ukhurebor KE, Obodo KO (2020) Removal of fluoride ions using a polypyrrole magnetic nanocomposite influenced by a rotating magnetic field. RSC Adv 10:595–609. https://doi.org/10.1039/C9RA07379E

61. El Nemr A, Shoaib AG, El Sikaily A, Mohamed AEDA, Hassan AF (2021) Evaluation of cationic methylene blue dye removal by high surface area mesoporous activated carbon derived from *Ulva lactuca*. Environ Process 8:311–332. https://doi.org/10.1007/s40710-020-00487-8

62. Hassaan MA, Hosny S, El-Katory MR, Ali RM, El Nemr A, Rangreez TA (2021) Dual action of both green and chemically synthesized zinc oxide nanoparticles: antibacterial activity and removal of Congo red dye. Desal Water Treat 218:423–435. https://doi.org/10.5004/dwt.2021.26988

63. El Nemr A, El-Sikaily A, Khaled A (2010) Modeling of adsorption isotherms of Methylene Blue onto rice husk activated carbon. Egypt J Aquatic Res 36(3):403–425

64. Salam MA, El-Shishtawy RM, Obaid AY (2014) Synthesis of magnetic multi-walled carbon nanotubes/magnetite/chitin magnetic nanocomposite for the removal of Rose Bengal from real and model solution. J Ind Eng Chem 20:3559–3567. https://doi.org/10.1016/j.jiec.2013.12.049

65. Sawood GM, Gupta SK (2020) Kinetic equilibrium and thermodynamic analyses of As (V) removal from aqueous solution using iron-impregnated Azadirachta indica carbon. Appl Water Sci 10:1–18. https://doi.org/10.1007/s13201-020-01217-z

66. Gupta P, Nagpal G, Gupta N (2021) Fly ash-based geopolymers: an emerging sustainable solution for heavy metal remediation from aqueous medium. Beni-Suef Univ J Basic Appl Sci 10:1–29. https://doi.org/10.1186/s43088-021-00179-8

67. Bullen J, Saleesongsom S, Weiss D (2020) A revised pseudo-second order kinetic model for adsorption, sensitive to changes in sorbate and sorbent concentrations. Chem Rxiv:PPR118372. https://doi.org/10.26434/chemrxiv.12008799.v1

68. Dada AO, Latona DF, Ojediran OJ, Nath OO (2016) Adsorption of Cu (II) onto bamboo supported manganese (BS-Mn) nanocomposite: effect of operational parameters, kinetic, isotherms, and thermodynamic studies. J Appl Sci Environ Managem 20:409–422. https://doi.org/10.4314/jasem.v20i2.24

69. Ebelegi AN, Ayawei N, Wankasi D (2020) Interpretation of adsorption thermodynamics and kinetics. Open J Phys Chem 10:166. https://doi.org/10.4236/ojpc.2020.103010

70. El Sikaily A, El Nemr A, Khaled A (2011) Copper sorption onto dried red alga Pterocladia capillacea and its activated carbon. Chem Eng J 168:707–714. https://doi.org/10.1016/j.cej.2011.01.064

71. Suteu D, Zaharia C, Badeanu M (2016) Kinetic modeling of dye sorption from aqueous solutions onto apple seed powder. Cell Chem Technol 50:1085–1091. https://doi.org/10.1205/095758298529326

72. Ismael MNM, El Nemr A, El Ashry ESH, Abdel Hamid H (2020) Removal of Hexavalent Chromium by Cross-Linking

Chitosan and N, N'-Methylene Bis-Acrylamide. Environ Process 7:911–930. https://doi.org/10.1007/s40710-020-00447-2

73. Girish CR, Murty VR (2016) Mass transfer studies on adsorption of phenol from wastewater using Lantana Camara, forest waste. Inter J Chem Eng Article ID 5809505 https://doi.org/10.1155/2016/5809505

74. Deghles A, Hamed O, Aza M, Lail BA, Azzaoui K, Obied AA, Jodeh S (2019) Cellulose with bidentate chelating functionality: an adsorbent for metal ions from wastewater. BioResources 14:6247–6266

75. Nworie FS, Nwabue FI, Oti W, Mbam E, Nwali BU (2019) Removal of methylene blue from aqueous solution using activated rice husk biochar: adsorption isotherms, kinetics and error analysis. J Chilean Chem Soc 64:4365–4376. https://doi.org/10.4067/s0717-97072019000104365

76. Oyelude EO, Awudza JA, Twumasi SK (2017) Equilibrium, kinetic and thermodynamic study of removal of eosin yellow from aqueous solution using teak leaf litter powder. Sci Rep 7:1–10. https://doi.org/10.1038/s41598-017-12424-1

77. Chittoo BS, Sutherland C (2019) Adsorption using lime-iron sludge–encapsulated calcium alginate beads for phosphate recovery with ANN-and RSM-optimized encapsulation. J Environ Eng 145:04019019. https://doi.org/10.1061/(ASCE)EE.1943-7870.0001519

78. El maguan Y, Elhadiri N, Benchanaa M, Chikri R (2020) Activated carbon for dyes removal: Modeling and understanding the adsorption process. J Chem 1–9: Article ID 2096834. https://doi.org/10.1155/2020/2096834

79. Singh PK, Banerjee S, Srivastava AL, Sharma YC (2015) Kinetic and equilibrium modeling for removal of nitrate from aqueous solutions and drinking water by a potential adsorbent, hydrous bismuth oxide. RSC Adv 5:35365–35376. https://doi.org/10.1039/c4ra11213j

80. Kuang Y, Zhang X, Zhou S (2020) Adsorption of methylene blue in water onto activated carbon by surfactant modification. Water 12:587. https://doi.org/10.3390/w12020587

81. El-Nemr MA, Yılmaz M, Ragab S, El Nemr A (2022) Biochar-SO Prepared from Pea Peels by Dehydration with Sulfuric Acid Improves the Adsorption of Cr^{6+} from Water. Biomass Conversion and Biorefinery In press. https://doi.org/10.1007/s13399-022-02378-4

82. Kyzioł-Komosińska J, Rosik-Dulewska C, Dzieniszewska A, Pająk M (2011) Compost as biosorbent for removal of acid dyes from the wastewater generated by the textile industry. Arch Environ Prot 37:3–14

83. Cuccarese M, Brutti S, De Bonis A, Teghil R, Mancini IM, Masi S, Caniani D (2021) Removal of diclofenac from aqueous solutions by adsorption on thermo-plasma expanded graphite. Scient Rep 11:3427. https://doi.org/10.1038/s41598-021-83117-z

84. Eleryan A, El Nemr A, Idris AM, Alghamdi MM, El-Zahhar AA, Said TO, Sahlabji T (2021) Feasible and eco-friendly removal of hexavalent chromium toxicant from aqueous solutions using chemically modified sugarcane bagasse cellulose. Toxin Rev 40(4):835–846. https://doi.org/10.1080/15569543.2020.1790606

85. Serag E, El-Maghraby A, Hassan N, El Nemr A (2021) CuO@ MWCNTs nanocomposite as non-enzyme electrochemical sensor for the detection of Malathion in seawater. Desal Water Treat 236:240–249. https://doi.org/10.5004/dwt.2021.27692

86. Helmy ET, El Nemr A, Gomaa E, El Dafrawy S, Mousa M (2021) Photocatalytic degradation of textile dyeing wastewater under visible light irradiation using green synthesized mesoporous nonmetal doped TiO_2. Bull Mater Sci 44:30. https://doi.org/10.1007/s12034-020-02322-0

87. Naji LA, Jassam SH, Yaseen MJ, Faisal AA, Al-Ansari N (2020) Modification of Langmuir model for simulating initial pH and temperature effects on sorption process. Sep Sci Technol 55:2729–2736. https://doi.org/10.1080/01496395.2019.1655055

88. Guo Y, Zhu Z, Qiu Y, Zhao J (2013) Enhanced adsorption of acid brown 14 dye on calcined Mg/Fe layered double hydroxide with memory effect. Chem Eng J 219:69–77. https://doi.org/10.1016/j.cej.2012.12.084

89. Khakyzadeh V, Rezaei-Vahidian H, Sediqi S, Azimi SB, Karimi-Nami R (2021) Programming Adsorptive removal of organic azo dye from aqueous media using magnetic carbon nano-composite. Chemical Methodologies 5:324–330. https://doi.org/10.22034/chemm.2021.131300

90. Ejikeme EM, Ejikeme PCN, Abalu BN (2014) Brown sea bean (Mucuna Sloanei) shell, an effective adsorbent for cationic dye removal. Inter J Eng Sci Res Tech 3:589–605

91. Valderrama C, Cortina JL, Farran A, Marti V, Gamisans X, Heras FDL (2008) Characterization of azo dye (Aacid Red 14) removal with granular activated carbon: equilibrium and kinetic data. Solvent Extr Ion Exch 26:271–288. https://doi.org/10.1080/07366290802053504

92. Valderrama C, Cortina JL, Farran A, Gamisans X, De Las Heras FX (2008) Evaluation of hyper-cross-linked polymeric sorbents (Macronet MN200 and MN300) on dye (Acid Red 14) removal process. React Funct Polym 68:679–691. https://doi.org/10.1016/j.reactfunctpolym.2007.11.005

Publisher's note Springer Nature remains neutral with regard to jurisdictional claims in published maps and institutional affiliations.

Authors and Affiliations

Tarek M. Eldeeb[1] · Uyiosa O. Aigbe[2] · Kingsley E. Ukhurebor[3] · Robert B. Onyancha[4] · Mohamed A. El-Nemr[5] · Mohamed A. Hassaan[1] · Otolorin A. Osibote[2] · Safaa Ragab[1] · Benedict Okundaye[6] · Vincent A. Balogun[7] · Ahmed El Nemr[1]

Tarek M. Eldeeb
tarikeldeeb77@yahoo.com

Uyiosa O. Aigbe
uyi4we@gmail.com

Kingsley E. Ukhurebor
ukeghonghon@gmail.com

Robert B. Onyancha
08muma@gmail.com

Mohamed A. El-Nemr
mohamedelnemr1992@yahoo.com

Mohamed A. Hassaan
mhss95@mail.com

Otolorin A. Osibote
osibotea@cput.ac.za

Safaa Ragab
safaa_ragab65@yahoo.com

Benedict Okundaye
benedictokundaye@yahoo.com

Vincent A. Balogun
vincent.balogun@edouniversity.edu.ng

[1] Environment Division, National Institute of Oceanography and Fisheries (NIOF), Kayet Bey, Elanfoushy, Alexandria, Egypt

[2] Department of Mathematics and Physics, Faculty of Applied Sciences, Cape Peninsula University of Technology, Cape Town, South Africa

[3] Department of Physics, Faculty of Science, Edo State University Uzairue, Edo State, Nigeria

[4] Department of Technical and Applied Physics, School of Physics and Earth Sciences Technology, Technical University of Kenya, Nairobi, Kenya

[5] Department of Chemical Engineering, Faculty of Engineering, Minia University, Minia, Egypt

[6] School of Art, Design, and Architecture, University of Huddersfield, Queensgate Huddersfield HD1 3DH, UK

[7] Department of Mechanical Engineering, Faculty of Engineering, Edo State University Uzairue, Edo State, Nigeria